Investigating brain connectivity heritability in a twin study using diffusion imaging data

K.-K. Shen[1], S. Rose[1], J. Fripp[1], K. L. McMahon[2], G. I. de Zubicaray[3],
N. G. Martin[4], P. M. Thompson[5], M. J. Wright[4], O. Salvado[1]

1. CSIRO Computational Informatics, Herston QLD 4029, Australia;
2. Centre for Advanced Imaging, University of Queensland, Brisbane, Australia;
3. School of Psychology, University of Queensland, Brisbane, Australia;
4. Queensland Institute of Medical Research, Brisbane, Australia;
5. Imaging Genetics Center, Institute for Neuroimaging & Informatics, University of South California, Los Angeles, CA, USA

Abstract

Heritability of brain anatomical connectivity has been studied with diffusion-weighted imaging (DWI) mainly by modeling each voxel's diffusion pattern as a tensor (e.g., to compute fractional anisotropy), but this method cannot accurately represent the many crossing connections present in the brain. We hypothesized that different brain networks (i.e., their component fibers) might have different heritability and we investigated brain connectivity using High Angular Resolution Diffusion Imaging (HARDI) in a cohort of twins comprising 328 subjects that included 70 pairs of monozygotic and 91 pairs of dizygotic twins. Water diffusion was modeled in each voxel with a Fiber Orientation Distribution (FOD) function to study heritability for multiple fiber orientations in each voxel. Precision was estimated in a test-retest experiment on a sub-cohort of 39 subjects. This was taken into account when computing heritability of FOD peaks using an ACE model on the monozygotic and dizygotic twins. Our results confirmed the overall heritability of the major white matter tracts but also identified differences inheritability between connectivity networks. Inter-hemispheric connections tended to be more heritable than intra-hemispheric and cortico-spinal connections.

Introduction

White matter (WM) structures develop and change throughout life. These changes are

influenced by both genetics and environment, and can be monitored using diffusion-weighted imaging (DWI) (Wozniak and Lim, 2006; Sullivan and Pfefferbaum, 2006, Cascio *et al*., 2007). Axon myelination is involved in the plasticity of cognitive functions, and may be altered by changes in myelin genes or mutation in neurological or psychiatric disorders (Fields, 2008). Based on the quantification of WM integrity using Diffusion Tensor Imaging (DTI), investigations into the heritability of WM structures usually estimate the genetic influence based on scalar measures such as fractional anisotropy (FA) or mean diffusivity (Jahanshad *et al*., 2013; for a review, see Kanchibhotla, *et al*., 2013). For example, the Tract-Based Spatial Statistics method revealed a significant genetic component influencing whole brain FA and radial diffusivity (Kochunov *et al*., 2010). Strong genetic influence on WM was shown at different stages of life (Pfefferbaum *et al*., 2001, Chiang *et al*., 2009, Brouwer *et al*. 2010).

DWI captures the complex microscopic features of axons, but a DTI model assumes a single dominant direction of water diffusion. This can be inadequate for representing voxels containing crossing or diverging fibers. New DWI techniques such as High Angular Resolution Diffusion Imaging (HARDI, Tuch *et al*., 2002) can resolve fiber microstructure more accurately. A voxel-wise diffusion orientation density function can be reconstructed by diffusion spectrum imaging (Lin *et al*., 2003), *q*-ball imaging (Tuch, 2004), or hybrid diffusion imaging (Zhan *et al*., 2011).

Our approach uses the Fiber Orientation Distribution technique (FOD, Tournier *et al*., 2004) to describe the intra-voxel structure of WM fibers. As the FOD is proportional to the fraction of fibers oriented along the respective direction, it can provide a biologically meaningful representation of the fiber structure in each voxel.

We hypothesized that there may be a different degree of genetic influence on distinct brain networks and their components. We investigated this hypothesis on a large cohort of

twins comprising 328 subjects that included 70 pairs of monozygotic (MZ) and 91 pairs of dizygotic (DZ) twins. We used FOD-based measurements to study crossing fibers individually and estimate genetic influences on intra-voxel fiber structures. A test-retest experiment was also conducted with repeated scans to evaluate the reliability of our image processing and analysis framework. We estimated the heritability of the FOD amplitudes, translating into heritability estimates for intra-voxel fiber populations, and estimated the average heritability along each tract by sampling the FOD. We further projected each tract's heritability onto the cortical areas it innervates, to study heritability pattern for various cortical networks. This links the heritability of WM organization with heritability patterns for cortical structure that have been reported before (Lenroot *et al*., 2009, Winkler *et al*., 2010, Joshi *et al*., 2011, Eyler *et al*., 2012). The overall heritability of the major WM tracts was high and we were also able to map some regional differences in heritability. In particular, inter-hemispheric connections tended to be more genetically influenced than intra-hemispheric and cortico-spinal connections.

Materials and Methods

Participants. The cohort consisted of 328 subjects (118M, 210F) with average age 22.7(2.3) years. Among the subjects, there were 71 pairs (*N*=142, 48M, 94F) of MZ twins with average age 22.8(2.2) years, and 90 pairs (*N*=180, 69M, 111F) of DZ twins with average age 22.6(2.4) years. A subset of 39 subjects (16M, 23F) with average age of 23.1(2.4) years was analyzed to estimate test-retest reliability. For this purpose, subjects were scanned twice at 3-month interval.

Image Acquisition. HARDI data were acquired using a 4T Bruker Medspec MRI scanner. Each dataset consisted of 11 images without diffusion sensitization (*b*=0), and diffusion weighted images (DWI) with 94 gradient directions at b = 1159s/mm^2.

Diffusion Magnetic Resonance (MR) Image Processing. The overall image processing pipeline is shown in Figure 1. The DWI images were pre-processed using point spread function mapping (Zaitsev *et al.*, 2004). The bias field was corrected using the N4 method (Tustison *et al.*, 2010). Interleaving artifacts due to subject motion within the same MR volume were corrected using the inverse interpolation method (Rohlfing *et al.*, 2008), and inter-volume motion was corrected by rigid registration of brain masks (Raffelt *et al.*, 2012). Image intensity was normalized across subjects (Raffelt *et al.*, 2012). Spherical harmonic deconvolution (Tournier *et al.*, 2008) was used to estimate the distribution of the fiber population in each voxel. In this approach, the observed HARDI signal in each voxel is modeled as a superposition of signals from the partial volumes of fibers aligned in various orientations. The fiber partial volume is modeled by a continuous distribution of fiber orientations. The sampled HARDI signal is estimated as a convolution of the FOD and the response signal from coherently aligned fibers (Leow *et al.*, 2009), and this was estimated from a region of interest in the corpus callosum defined on the common atlas.

Spatial normalization of FOD images to a common atlas space. Once corrected, all the subjects' datasets were aligned to a common template (Figure 1). We created an atlas from the data set by iteratively computing a non-rigid registration of each subject to the current template, followed by averaging all the subjects' transformed data to estimate a new template. At the first iteration a randomly chosen subject was used as the template. The non-rigid registration was performed on the FOD images using a symmetric diffeomorphic registration (Raffelt *et al.*, 2011). Briefly, during registration the FOD of each voxel represented by spherical harmonic coefficients was interpolated using B-spline interpolation once the image was warped to the template. Besides interpolation, the spatial transformation was also used to modify each FOD to reorient the fiber population within each voxel. Each FOD was reoriented by an affine transformation that approximated the local deformation field. In

addition, to correct for the local deformation of the transformation field, a modulation step was required. The FOD amplitude in each spatial orientation was rescaled by a modulation factor computed from the local Jacobian (Raffelt *et al*., 2012).

After the final iteration, the template represented the sample average with each voxel modeled as the average of all the subjects. An FA map was computed using a tensor model for each subject. The same transformation field for each subject was also used to transform the FA map of each subject and to create an average FA map. By registering the average FA map to the FA map from the JHU DTI atlas (Mori *et al*., 2005, Wakana *et al*., 2007, Hua *et al*., 2008), we realigned the FOD maps for each subject to the standard MNI coordinates with a dense spatial correspondence between the sampled population and the MNI space.

Detection of the FOD peaks. Once all the subjects' images had been spatially normalized to the common template, voxel-wise statistical analysis was performed (Figure 1). As the FOD describes the distribution of underlying WM fibers within the voxel, the amplitude of the FOD peaks estimates the proportion of axons aligned in different orientations (Raffelt *et al*., 2012). We measured the amplitude of the FOD peaks, and used this to estimate a measure of WM heritability. The three principal FOD peak amplitudes were estimated in each voxel of the average FOD template using MRtrix (Tournier *et al*., 2012). The same estimate for each subject also yielded three main FOD peaks in each voxel, which were matched to the most likely peaks from the template, based on angular error. Finally, for each voxel, the three FOD peak amplitudes were ranked and the two largest used in analyses described below, unless the second highest FOD peak was lower than 0.1, in which case only one FOD peak was considered (Jeurissen *et al*., 2013).

Statistical analysis. Voxel-based analysis was performed on the FOD peak amplitude (i.e., two peaks or one depending on the previous step). Test-retest reliability (precision) of the FOD peaks' amplitude was estimated for each voxel. We computed the average the reliability

of the largest two FOD peaks, respectively, over the WM regions of interest (ROI) according to the probabilistic JHU DTI tractography atlas (Hua *et al.*, 2008) in which the ROIs defined by probability greater than 25% (Jahanshad *et al.*, 2010) were used. Subdivisions of corpus callosum and internal capsule were also included using the JHU ICBM labels (Wakana *et al.*, 2007).

To estimate the reliability of the MR diffusion measurements, we compared images of the same subjects at two different time points. We used the intraclass correlation (ICC, Shrout and Fleiss, 1979) to evaluate the test-retest reliability of the FOD peak amplitudes. The ICC was calculated for each of the FOD peak amplitudes in each voxel, and was defined as:

$$\text{ICC} = \frac{\text{BMS} - \text{WMS}}{\text{BMS} + \text{WMS}}$$

where BMS is the between-subject mean square variance, and WMS is the mean square variance within the subject between test and retest time points. Negative ICC estimates were clamped to zero (Bartko, 1976), such that the variance remained non-negative, consistent with ICC interpretation. Measurements were inverse-normalized and corrected for age and sex.

One can expect the relative influence of genetic and environmental factors to be different among MZ twins and DZ twins as MZ twins share identical genes whereas DZ twins share on average only half of their genes. Using an ACE model, FOD peak amplitudes were assumed to be subject to the influence of three factors: additive genetics A, common environment C, and residual E due to unique environment and measurement errors which are independent between individuals. We thus assumed that

$$\text{FOD}_{\text{peak}} = A + C + E.$$

The measurements of FOD peak amplitude were used to fit the covariance structure of the

ACE model. A non-negative least squares estimation (Lawson and Hanson, 1987, Chen *et al*., 2013) was used to estimate the variance of each component and the heritability index estimates for additive genetic influences, within the total variance defined as:

$$h^2 = \frac{\mathrm{Var}(A)}{\mathrm{Var}(\mathrm{FOD_{peak}})}.$$

A likelihood ratio test (LRT) comparing the ACE model and CE model of the environment factors only (i.e. common environment *C* and unique environment *E*) was used to assess the significance of the additive genetic component *A* for each FOD peak. The *p*-value of the LRT was computed by 1000 permutations.

Tract-based analysis. A diagram illustrating our tract-based analysis is shown in Figure 2. We first performed whole brain probabilistic fiber tracking (Tournier *et al*., 2012) on the population average FOD template, creating a tractogram. Only the tracts connecting the cortical mantle (gray matter, GM), linking cerebral cortex with subcortical nuclei, such as cortico-striatal and cortico-thalamic tracts, and those travelling through the brain stem were kept. All other tracts were excluded as they do not represent anatomically plausible pathways. Voxels with FA > 0.3 in the average template, and voxels most probably containing WM (as opposed to GM and cerebrospinal fluid) according to the *a priori* probability of the ICBM 152 atlas (Fonov *et al*., 2011) were delineated as the WM ROI. The cerebral cortex and subcortical nuclei were parcellated using the Anatomical Automatic Labeling atlas (AAL, Tzourio-Mazoyer, 2002), and the brain stem mask was defined as in the Harvard-Oxford atlas (Markis *et al*., 2006).

We assumed that FOD peaks characterized the underlying fiber structure in each voxel, and thus the heritability FOD peaks described genetic influence on the fiber tracts travelling through the voxel along the direction of the FOD peaks. This allowed us to project the test-retest reliability ICC and heritability index h^2 of FOD peaks onto each of the fiber

tracts in the tractogram. To do so, ICC and h^2 were computed on each tract at points sampled by the fiber tracking algorithm at a step size of 0.2 mm along its path, interpolated using the eight surrounding voxels. In the surrounding voxels with two FOD peaks, we chose the peak that had the smaller angle difference with the tangent of the tract at the sample location. The interpolating weight for each peak was determined in the same way as in bilinear image interpolation. In cases where the angles between the tangential direction of the tract at a point and all peak directions in one of the neighboring voxels were greater than 45 degrees, we assigned zero reliability and zero heritability to the peak in the interpolation. This penalized the tracts deviating from the FOD peak directions by reducing their contributions. In addition, h^2 estimates were further filtered by keeping only those directions with an ICC greater or equal than 0.6.

To characterize the reliability and heritability of each tract, we used the trimmed mean over the entire stretch of the tract, removing extreme values due to large deviation away from the FOD peak directions or low reliability. The trimmed mean was computed by removing the 5% highest and the 5% lowest values. This enabled us to rank and select the tracts based on the average reliability of the FODs they travel through, or the average genetic influence expressed upon them.

Linking white matter fibers with cortical regions. By associating the tracts with the cortical regions that they connect to, we were able to relate genetic influences on the WM connections with subdivisions of the cortex. The cortex may be parcellated into a number of ROIs, or cortical patches, according to various definitions. Here we used the AAL atlas, described above. We identified the subset of tracts from the tractogram that ended in each cortical ROI. From this subset, a heritability distribution was estimated (i.e., for each ROI we computed a histogram). For each ROI, the heritability distribution was binned to study the proportion of tracts with various heritability ranges, in addition to reporting the heritability

average that could be color-coded over the brain surface for each patch.

The histogram of the heritability was bimodal for most of the ROIs. We thus fitted a sum of two normal distributions using the Expectation-Maximization algorithm (McLachlan and Peel, 2000). The two normal distributions were separated by applying a minimal error threshold (Kittler and Illingworth, 1986), resulting in two fiber bundles originating from each ROI. The number of fiber tracts in the tractogram is not guaranteed to be proportional to the number of axons. The measures of mean heritability and percentage of heritable fiber tracts in each cortical ROI are thus not strictly quantitative. Therefore, the size of each component in the bimodal Gaussian mixture may not reflect the distribution of heritability in the axon population. Nevertheless, it may indicate distinct and spatially separable bundles sharing the same cortical region while displaying different levels of genetic influence.

Results

The entire cohort (N=328, repeated scans not included) was first used to build a population-specific FOD atlas, and this was used as a template for the spatial normalization of the diffusion MR images. Among the 328 subjects, 322 subjects are twin pairs comprising 71 MZ twins and 90 DZ twins. The component corresponding to the zero[th] order spherical harmonic (SH) coefficient of the average FOD for that template is shown in Figure 3. The deformation fields generated to build that template were used to non-rigidly register all the subject's images, including FOD reorientation and modulation. The 78 scans corresponding to the 39 test-retest subjects were registered independently in the same way. The cohort used for the heritability experiments comprised 322 FOD images of twins.

Reliability of FOD peak measures

To visualize results, the test-retest ICC of FOD peak amplitude was plotted on the average FOD template. For each voxel FOD, the "cap" of its peaks was color-coded according to the

ICC value of each peak. A close-up view of the coronal section with crossing fibers of the *corona radiata* is shown in Figure 4, where the two main peaks of FODs with fibers crossing can be seen.

To investigate precision, a test-retest ICC map was created corresponding to the first FOD peak in the WM region (Figure 5). The average of estimated test-retest ICC in the WM was 0.670. The test-retest ICC for voxels with a second peak (FOD > 0.1) is shown in Figure 6. The ICC average was 0.547 for the second peak. ROI based analysis was carried out using the labeling from the JHU DTI atlas. The average test-retest ICC in each ROI is listed in Figure 7.

Heritability of WM measured by FOD peak

The heritability index h^2 for the first FOD peak in WM is shown in Figure 8. After applying the binary mask to suppress less reliable estimates (ICC < 0.6), the heritability of the first FOD peak averaged over the entire WM region was 0.194. Significant component of additive genetic influence was found in major WM tracts, where the average over all the major WM tracts defined in the JHU atlas was 0.291. The results for the second FOD peak are shown in Figure 9, and the average within the WM was 0.129.The average heritability of WM in each ROI of the JHU atlas is listed in Figure 10.

Relatively high heritability was found for the corpus callosum, where the average heritability of the FOD peak was 0.552 in the body, 0.519 in the genu, and 0.499 in the splenium. The left and right inferior fronto-occipital fasciculus had a heritability of 0.347 and 0.381, respectively. The superior longitudinal fasciculus (h^2: left 0.307, right 0.381) and the inferior longitudinal fasciculus (h^2: left 0.204, right 0.259) were found to be less heritable. The heritability of FOD peak measurements in cortico-spinal tracts were estimated to be 0.287 (left) and 0.418 (right) along the tracts.

For areas known to include crossing fibers such as the *corona radiata* (labeled as cortico-spinal tract in the ROI definition), moderate heritability of the second FOD peak was found (left 0.232, right 0.220). There was also a moderately heritable component found in the second FOD peaks in the superior longitudinal fasciculus (left 0.155, right 0.179) in addition to more pronounced heritability in the first peak (left 0.307, right 0.381).

Heritable WM fiber tracts

We built a whole brain tractogram on the population average FOD template using a probabilistic fiber tracking algorithm. In total 250,000 tracts were generated, among which 122,000 were kept because both ends were located in the cortex, connecting to subcortical nuclei, or passing through the brain stem. We selected among these tracts a reliable subset with track-average test-retest ICC greater than 0.6, comprising 98,000 tracts, which were then ranked according to their average heritability index, h^2. Projections of the tractogram are shown in Figure 11, which shows the reliable subset of tracts from the fiber tracking algorithm, and the tracts with average heritability greater than 0.45. In Figure 12, the tractogram was binned into 6 classes according to h^2, showing the WM fiber tracks with heritability ranging from below 0.2 to greater than 0.45.The fibers with different heritability appeared to form different connection networks. For instance, in Figure 12, the less heritable fiber connections are almost absent in the corpus callosum, whereas the commissural fibers transiting via the corpus callosum appeared exclusively in groups with higher heritability.

Cortical regions linked to heritable WM tracks

Figure 13 shows the results after mapping the average heritability along each tract on the cortical surface where it connects. In addition, for each cortical ROI defined by the AAL atlas, we plotted the mean heritability of all of the tracts originating or ending in that ROI (Figure 13a). We also plotted the percentage of tracks terminating in each ROI that were

found to be heritable at the level $h^2 > 0.3$ and $h^2 > 0.4$ (Figure 13b—c).

The average heritability of tracts ending in the medial superior frontal gyri (left and right), medial orbitofrontal gyri (left and right), right paracentral lobule, and right hippocampus was greater than 0.3. A substantial subpopulation of fiber tracks ($> 10\%$) ending in the left superior frontal gyrus, medial superior frontal gyri (left and right), medial orbitofrontal gyri (left and right), right hippocampus, right posterior cingulum had a heritability greater than 0.4. Heritable fibers ($h^2 > 0.4$) were also found to connect to right post-central gyrus, precuneus cortices (left and right), cingulate gyri (left and right), left middle frontal gyrus, and right calcarine sulcus.

Examining the distribution of heritability of WM fiber tracks connected to each cortex area, we found that the fiber tracks ending in bilateral superior frontal gyrus, supplementary motor area, middle frontal gyrus, and left cingulate gyrus displayed a bimodal distribution. By performing a cluster analysis we identified two distinct subpopulations of WM fibers with different heritabilities. The distributions of WM heritability in tracts projecting from these cortical regions are shown in Figure 14, along with the tracts in each component forming bundles separated by the minimal error threshold.

Discussion

We investigated the heritability of brain connectivity in a twin cohort using a FOD model that allows us to study crossing pathways in the brain. We estimated the heritability of WM using the FOD peak amplitude and evaluated its precision by a test-retest experiment. The FOD peaks had a heritability h^2~0.3 on average over the major WM tracts. More specifically, the commissural connection between contralateral hemispheres showed greater heritability than intra-hemispheric and cortico-spinal connections. The mostly highly heritable tracts connected particular cortical regions, especially the medial frontal cortices and right

hippocampus. For tracts that terminated in cortical regions such as the supplementary motor area and cingulate gyri, the precentral gyri, and the superior frontal gyri, a bimodal distribution of tract heritability was observed. Fibers with higher heritability formed bundles connecting mostly to the contralateral hemisphere.

Reliability of FOD peak measures

The reproducibility of diffusion MR image using DTI-based metrics such as FA and diffusivity was studied mainly through ROI-based analyses (for a review see Vollmar *et al*., 2010). Voxel-wise analysis of FA was conducted by Farrell *et al*. (2007). The precision of FOD peak orientation was evaluated both by simulation and on *in vivo* data (Tournier *et al*., 2007, Tournier *et al*., 2008). In our analysis framework several sources of error leading to inter-scan variability are present. They include CSD reconstruction, image registration, peak identification and matching. The modulation of FOD in the spatial normalization may also introduce extra inter-scan variance. We tried to measure this variability by performing a test-retest experiment and taking it into account when estimating heritability. ICC compares the variance due to measurement itself with the variance among a healthy population. By restricting to measurements with ICC over 0.6, we considered only consistent and replicable measurements of fiber density in WM regions. However ICC is not related to accuracy, only to precision, so results might be consistently wrong.

Figure 8 reveals a pattern of higher heritability in the centre of the brain (h^2~0.6) that decreased towards the cortex (h^2~0.2). This pattern is also observed in the ICC maps suggesting a lower precision in those areas towards the cortex, which is consistent with the inter-individual variability in gyral folding that is influenced by non-genetic factors (Bartley *et al*., 1997, Biondi *et al*., 1998).

Two limitations of our study were inherent to the acquisition protocol: lack of a field

map to fully correct for susceptibility-related distortion and a DWI parameter of b=1159mm/s^2 which is not the optimal value for computing the FOD model. Despite those, we believe that our findings still provide interesting insights into the heritability of brain connectivity.

WM tract heritability

FOD peak amplitude displays high heritability across major WM tracts. In particular, for the corpus callosum, cortico-spinal tracts, the inferior fronto-occipital fasciculus, and the superior longitudinal fasciculus, it shows how FOD-based measures can capture the genetic effects on WM structures. The detected heritability was rather conservative since the heritability of FOD peaks with low reliability was not considered. We might have underestimated heritability in fibers passing through these voxels. The results with lower heritability should be interpreted cautiously: a low heritability estimate may not necessarily suggest strong environmental influences, but low precision estimated from the test-retest. However, when all WM voxels were included (including those with low precision), similar qualitative results were observed (not shown).

The corpus callosum communicates between both sides of the brain. The high heritability of WM measures along the corpus callosum suggests a strong influence of genes upon the inter-hemisphere connection. Corpus callosum growth continues into adulthood (Pujol *et al*., 1993, Luders *et al*., 2010, Paul, 2011), which is guided and regulated by a wide range of genes and environmental factors (Paul *et al*., 2007). Our finding of highly heritable corpus callosum is consistent with DTI-based findings suggesting that WM integrity is under heavy genetic influence in the corpus callosum (Pfefferbaum *et al*., 2001, Chiang *et al*., 2009, Brouwer *et al*., 2010). Voxel-based morphometry found strong genetic contributions to WM density in corpus callosum (Hulshoff Pol *et al*., 2006), results that we confirmed, observing the highest heritability in the genu of corpus callosum. This area showed high heritability

regardless of imaging protocol (Jahanshad *et al.*, 2012). In the posterior parts of the corpus callosum, a pattern of more rapid growth during the development has been reported (Rajapakse *et al.*, 1996, Giedd *et al.*, 1999, Thompson *et al.*, 2000, Chung *et al.*, 2001); these regions displayed lower heritability using our method, compared to the anterior parts.

In the superior frontal gyrus, middle frontal gyrus, the middle part of the cingulate gyrus and supplementary motor area, the fiber cluster with higher average heritability corresponded to bundles connecting these cortices to the contralateral hemisphere. For instance, in the left supplementary motor area, the heritability of tracts connected to this part of the cortex distinctly formed a bimodal distribution. A majority of tracts along the ipsilateral projection or association was less heritable, but the commissural connection had a higher heritability consistent with the high heritability in the corpus callosum.

The heritabilities for the inferior fronto-occipital fasciculus and the superior longitudinal fasciculus were relatively high, whereas the inferior longitudinal fasciculus was lower. These former structures are significantly influenced by genetic effects in DTI studies (Chiang *et al.*, 2009, Kochunov *et al.*, 2010, Brouwer *et al.*, 2010). High heritability has been reported in the right superior longitudinal fasciculus (Brouwer *et al.*, 2010), consistent with our findings. The genetic influences on the superior longitudinal fasciculus are shared with performance measures of a spatial delayed response task (Karlsgodt *et al.*, 2010).

Among the tracts ending in the orbitofrontal cortex, a bimodal distribution in heritability was observed. The cluster with higher heritability (usually $h^2>0.3$) included the inter-hemisphere connections in the *forceps minor* and the inferior fronto-occipital fasciculi connecting the orbital surface.

Genetic specifications are critical to the early development of the cortico-spinal system, which plays an important role in the control of skilled limb movements. Its

maturation and the long-term function of the motor system also depend on activity and experience (Martin *et al*., 2007). Cortico-spinal tracts descending from motor cortex through the posterior limb of internal capsule to the spinal cord were heritable ($h^2 > 0.3$), as in previous studies (Hulshoff Pol *et al*., 2006). In the anterior limb of internal capsule, WM integrity measured by FA was under strong genetic control bilaterally (Chiang *et al*., 2009). In our results, high heritability was found in the right anterior limb of the internal capsule, whereas in the left anterior limb the heritability was limited by voxels with lower test-retest reliability (<0.6).

Cortices linked to heritable WM tracts

A variety of cortical areas have been found to be heritable in several morphological studies (Thompson *et al.* 2001, Hulshoff Pol *et al*., 2006), with more specific genetic influences found for cortical surface area (Panizzon *et al*., 2009, Eyler *et al*., 2011), and cortical thickness (Lenroot *et al*., 2009, Winkler *et al*., 2010, Joshi *et al*., 2011). An inverse relationship was found between cortical thickness and WM growth (Sowell *et al*., 2001; Gogtay *et al*., 2004, Giorgio *et al*., 2009). Schmitt *et al.* (2008) related the network organization to the cortical parcellation using principal component analysis, where the first principal component accounted for over 60% of the total covariance in genetic influence among all cortical regions. In this paper, we mapped the heritability in WM connections to the cortex. By examining which cortical regions were connected by heritable tracts, the function associated with cortices may shed light on the significance of genetic effects for particular WM structures.

In our results, the heritability for fibers projecting to the superior and middle frontal gyrus, and the middle temporal gyrus is consistent with previous findings reporting GM volume or thickness heritability in those areas (Thompson *et al*., 2001, Hulshoff Pol *et al*., 2006, Elyer *et al*., 2011). The primary somatosensory cortex in the postcentral gyrus and the

paracentral lobule adjacent to it were connected to heritable WM. The development of this cortical region was phylogenetically and ontologically early, and genetically determined (Lenroot *et al.*, 2009). The medial prefrontal cortex in the contralateral hemisphere is connected via the genu of corpus callosum. Given the high heritability in the genu, fibers projecting to medial prefrontal cortex showed higher heritability. A heritability h^2=0.83 was found for GM density in the medial frontal cortex (Hulshoff Pol *et al.*, 2006), which agrees with previous findings (Thompson *et al.*, 2001). Commissural connections projecting to the cingulate gyrus, especially its posterior part, via the corpus callosum also contributed to a substantial subpopulation of heritable tracts. Cortical GM areas corresponding to the hippocampus and caudate were also connected by heritable fibers (h^2>0.4, Figure 13c).

In conclusion, we report a new method to investigate the heritability of brain connections using DWI data with an FOD model. Our findings are consistent with prior studies and offer a novel way to investigate complex brain networks involving crossing fibers. They suggest that inter-hemisphere connections are more heritable than association and cortico-spinal connections.

Acknowledgement

References

Aganj I, Lenglet C, Sapiro G, Yacoub E, Ugurbil K, Harel N (2010) Reconstruction of the orientation distribution function in single- and multiple-shell q-ball imaging within constant solid angle. Magnetic Resonance in Medicine 64: 554–566.

Bartko JJ (1976) On various intraclass correlation reliability coefficients. Psychological

Bulletin 83: 762–765.

Bartley AJ, Jones DW, Weinberger DR (1997) Genetic variability of human brain size and cortical gyral patterns. Brain 120: 257–269.

Besseling RMH, Jansen JFA, Overvliet GM, Vaessen MJ, Braakman HMH, Hofman PAM, Aldenkamp AP, Backes WH (2012) Tract Specific Reproducibility of Tractography Based Morphology and Diffusion Metrics PLoS ONE 7: e34125.

Biondi A, Nogueira H, Dormont D, Duyme M, Hasboun D, Zouaoui A, Chantôme M, Marsault C (1998) Are the brains of monozygotic twins similar? A three-dimensional MR study. Am J Neuroradiol 19: 1361–1367.

Bisdas S, Bohning De, Bešenski N, Nicholas, JS, Rumboldt Z (2008) Reproducibility, Interrater Agreement, and Age-Related Changes of Fractional Anisotropy Measures at 3T in Healthy Subjects: Effect of the Applied b-Value. Am J Neuroradiol 29: 1128–1133.

Bonekamp D, Nagae LM, Degaonkar M, Matson M, Abdalla WMA, Barker PB, Mori S, Horská A (2007) Diffusion tensor imaging in children and adolescents: Reproducibility, hemispheric, and age-related differences. NeuroImage 34: 733–742.

Brouwer RM, Mandl RCW, Peper JS, van Baal GCM, Kahn RS, Boomsma DI, Hulshoff Pol HE (2010) Heritability of DTI and MTR in nine-year-old children. NeuroImage 53: 1085–1092.

Brown TT, Jernigan TL (2012) Brain Development During the Preschool Years. Neuropsychol Rev 22: 313–333.

Canales-Rodríguez EJ, Melie-García L, Iturria-Medina Y (2009) Mathematical description of q-space in spherical coordinates: Exact q-ball imaging. Magnetic Resonance in Medicine 61: 1350–1367.

Cascio CJ, Gerig G, Piven J (2007) Diffusion Tensor Imaging: Application to the Study of the Developing Brain. Journal of the American Academy of Child & Adolescent Psychiatry 46: 213–223.

Chiang M-C, Barysheva M, Shattuck DW, Lee AD, Madsen SK, Avedissian C, Klunder AD, Toga AW, McMahon KL, de Zubicaray GI, Wright MJ, Srivastava A, Balov N, Thompson PM (2009) Genetics of Brain Fiber Architecture and Intellectual Performance. J Neurosci 29: 2212–2224.

Chung MK, Worsley KJ, Paus T, Cherif C, Collins DL, Giedd JN, Rapoport JL, Evans AC (2001) A Unified Statistical Approach to Deformation-Based Morphometry. NeuroImage 14: 595–606.

Chen X, Blokland G, Strike L (2013) Voxel-wise and cluster-based heritability inferences of fMRI data. In: Organization of Human Brain Mapping, Seattle, WA.

Ciccarelli O, Parker GJ, Toosy AT, Wheeler-Kingshott CA, Barker GJ, Boulby PA, Miller DH, Thompson AJ (2003) From diffusion tractography to quantitative white matter tract measures: a reproducibility study. NeuroImage 18: 348–359.

Descoteaux M, Angelino E, Fitzgibbons S, Deriche R (2007) Regularized, fast, and robust analytical Q-ball imaging. Magnetic Resonance in Medicine 58: 497–510.

Eyler LT, Prom-Wormley E, Panizzon MS, Kaup AR, Fennema-Notestine C, Neale MC, Jernigan TL, Fischl B, Franz CE, Lyons MJ, Grant M, Stevens A, Pacheco J, Perry ME, Schmit JEt, Seidman LJ, Thermenos HW, Tsuang MT, Chen C-H, Thompson WK, Jak A, Dale AM, Kremen WS (2011) Genetic and Environmental Contributions to Regional Cortical Surface Area in Humans: A Magnetic Resonance Imaging Twin Study. Cereb Cortex 21: 2313–2321.

Farrell JAD, Landman BA, Jones CK, Smith SA, Prince JL, van Zijl PCM, Mori S (2007)

Effects of signal-to-noise ratio on the accuracy and reproducibility of diffusion tensor imaging–derived fractional anisotropy, mean diffusivity, and principal eigenvector measurements at 1.5T. Journal of Magnetic Resonance Imaging 26: 756–767.

Fields RD (2008) White matter in learning, cognition and psychiatric disorders. Trends in Neurosciences 31: 361–370.

Fonov V, Evans AC, Botteron K, Almli CR, McKinstry RC, Collins DL (2011) Unbiased average age-appropriate atlases for pediatric studies. NeuroImage (2011): 313–327.

Giannelli M, Cosottini M, Michelassi MC, Lazzarotti G, Belmonte G, Bartolozzi C, Lazzeri M (2010) Dependence of brain DTI maps of Fractional Anisotropy and Mean Diffusivity on the number of diffusion weighting directions. Journal of Applied Clinical Medical Physics 11: 176–190.

Giedd JN, Blumenthal J, Jeffries NO, Rajapakse JC, Vaituzis AC, Liu H, Berry YC, Tobin M, Nelson J, Castellanos FX (1999) Development of the human corpus callosum during childhood and adolescence: A longitudinal MRI study. Progress in Neuro-Psychopharmacology and Biological Psychiatry 23: 571–588.

Geng X, Prom-Wormley EC, Perez J, Kubarych T, Styner M, Lin W, Neale MC, Gilmore JH (2012) White Matter Heritability Using Diffusion Tensor Imaging in Neonatal Brains. Twin Research and Human Genetics 15: 336–350.

Giorgio A, Watkins KE, Chadwick M, James S, Winmill L, Douaud G, De Stefano N, Matthews PM, Smith SM, Johansen-Berg H, James AC (2010) Longitudinal changes in grey and white matter during adolescence. NeuroImage 49: 94–103.

Gogtay N, Giedd JN, Lusk L, Hayashi KM, Greenstein D, Vaituzis AC, Nugent Tf, Herman DH, Clasen LS, Toga AW, Rapoport JL, Thompson PM (2004) Dynamic mapping of human cortical development during childhood through early adulthood. Proc Natl Acad Sci 101:

8174–8179.

Hakulinen U, Brander A, Ryymin P, Öhman J, Soimakallio S, Helminen M, Dastidar P, Eskola H (2012) Repeatability and variation of region-of-interest methods using quantitative diffusion tensor MR imaging of the brain. BMC Med Imaging 12: 30.

Heiervang E, Behrens TEJ, Mackay CE, Robson MD, Johansen-Berg H (2006) Between session reproducibility and between subject variability of diffusion MR and tractography measures. NeuroImage 33: 867–877.

Hua K, Zhang J, Wakana S, Jiang H, Li X, Reich DS, Calabresi PA, Pekar JJ, van Zijl PCM, Mori S (2008) Tract probability maps in stereotaxic spaces: Analyses of white matter anatomy and tract-specific quantification. NeuroImage 39: 336–347.

Huang L, Wang X, Baliki MN, Wang L, Apkarian AV, Parrish TB (2012) Reproducibility of Structural, Resting-State BOLD and DTI Data between Identical Scanners. PLoS ONE 7: e47684.

Hulshoff Pol HE, Schnack HG, Posthuma D, Mandl RCW, Baaré WF, van Oel C, van Haren NE, Collins DL, Evans AC, Amunts K, Bürgel U, Zilles K, de Geus E, Boomsma DI, Kahn RS (2006) Genetic Contributions to Human Brain Morphology and Intelligence. J Neurosci 26: 10235–10242.

Jahanshad N, Lee AD, Barysheva M, McMahon KL, de Zubicaray GI, Martin NG, Wright MJ, Toga AW, Thompson PM Genetic influences on brain asymmetry: A DTI study of 374 twins and siblings. NeuroImage 52: 455–469.

Jahanshad N, Kohannim O, Toga AW, McMahon KL, de Zubicaray GI, Hansell NK, Montgomery GW, Martin NG, Wright MJ, Thompson PM (2012) Diffusion Imaging Protocol Effects on Genetic Associations. In: Proceedings / IEEE International Symposium on Biomedical Imaging: from nano to macro. IEEE International Symposium on Biomedical

Imaging, pp. 944–947.

Jahanshad N, Kochunov PV, Sprooten E, Mandl RC, Nichols TE, Almasy L, Blangero J, Brouwer RM, Curran JE, de Zubicaray GI, Duggirala R, Fox PT, Hong LE, Landman BA, Martin NG, McMahon KL, Medland SE, Mitchell MD, Olvera RL, Peterson CP, Starr JM, Sussmann JE, Toga AW, Wardlaw JM, Wright MJ, Hulshoff Pol HE, Bastin ME, McIntosh AM, Deary IJ, Thompson PM, Glahn DC (2013) Multi-site genetic analysis of diffusion images and voxelwise heritability analysis: A pilot project of the ENIGMA–DTI working group. NeuroImage 81: 455–469.

Jansen JFA, Kooi ME, Kessels AGH, Nicolay K, Backes WH (2007) Reproducibility of Quantitative Cerebral T2 Relaxometry, Diffusion Tensor Imaging, and 1H Magnetic Resonance Spectroscopy at 3.0 Tesla. Investigative Radiology 42: 327–337.

Jeurissen, B, Leemans, A, Tournier, J-D, Jones, DK, Sijbers, J (2013) Investigating the prevalence of complex fiber configurations in white matter tissue with diffusion magnetic resonance imaging. Human Brain Mapping 34:2747–2766.

Jones DK (2004) The effect of gradient sampling schemes on measures derived from diffusion tensor MRI: a Monte Carlo study. Magn Reson Med 51: 807–815.

Joshi AA, Leporé N, Joshi SH, Lee AD, Barysheva M, Stein JL, McMahon KL, Johnson K, de Zubicaray GI, Martin NG, Wright MJ, Toga AW, Thompson PM (2011) The contribution of genes to cortical thickness and volume. NeuroReport 22: 101–105.

Karlsgodt KH, Kochunov P, Winkler AM, Laird AR, Almasy L, Duggirala R, Olvera RL, Fox PT, Blangero J, Glahn DC (2010) A Multimodal Assessment of the Genetic Control over Working Memory. J Neurosci 30: 8197–8202.

Kanchibhotla SC, Mather KA, Wen W, Schofield PR, Kwok JBJ, Sachdev PS (2013) Genetics of ageing-related changes in brain white matter integrity – A review. Ageing

Research Reviews 12: 391–401.

Kittler J, Illingworth J (1986) Minimum error thresholding. Pattern Recognition 19: 41–47.

Kochunov O, Glahn DC, Lancaster JL, Winkler AM, Smith S, Thompson PM, Almasy L, Duggirala R, Fox PT, Blangero J (2010) Genetics of microstructure of cerebral white matter using diffusion tensor imaging. NeuroImage 53: 1109–1116.

Landman BA, Farrell JAD, Jones CK, Smith SA, Prince JL, Mori S (2007) Effects of diffusion weighting schemes on the reproducibility of DTI-derived fractional anisotropy, mean diffusivity, and principal eigenvector measurements at 1.5T. NeuroImage 36: 1123–1138.

Lawson CL, Hanson RJ (1995) Solving least squares problems. Philadelphia: SIAM.

Lenroot RK, Schmitt JE, Ordaz SJ, Wallace GL, Neale MC, Lerch JP, Kendler KS, Evans AC, Giedd JN (2009) Differences in genetic and environmental influences on the human cerebral cortex associated with development during childhood and adolescence. Human Brain Mapping 30: 163–174.

Leow AD, Zhu S, Zhan L, McMahon K, de Zubicaray GI, Meredith M, Wright MJ, Toga AW, Thompson PM (2009) The tensor distribution function. Magnetic Resonance in Medicine 61: 205–214.

Lin C-P, Wedeen VJ, Chen J-H, Yao C, Tseng W-YI (2003) Validation of diffusion spectrum magnetic resonance imaging with manganese-enhanced rat optic tracts and ex vivo phantoms. NeuroImage 19: 482–495.

Luders E, Thompson PM, Toga AW (2010) The Development of the Corpus Callosum in the Healthy Human Brain. J Neurosci 30: 10985–10990.

Makris N, Goldstein JM, Kennedy D, Hodge SM, Caviness VS, Faraone SV, Tsuang MT,

Seidman LJ (2006) Decreased volume of left and total anterior insular lobule in schizophrenia. Schizophrenia Research 83: 155–171.

Martin JH, Friel KM, Salimi I, Chakrabarty S (2007) Activity- and use-dependent plasticity of the developing corticospinal system. Neuroscience & Biobehavioral Reviews 31: 1125–1135.

McLachlan GJ, Peel D (2000) Finite mixture models. New York: Wiley.

Muetzel RL, Collins PF, Mueller BA, Schissel AM, Lim KO, Luciana M (2008) The development of corpus callosum microstructure and associations with bimanual task performance in healthy adolescents. NeuroImage 39: 1918–1925.

Panizzon MS, Fennema-Notestine C, Eyler LT, Jernigan TL, Prom-Wormley E, Neale M, Jacobson K, Lyons MJ, Grant MD, Franz CE, Xian H, Tsuang M, Fischl B, Seidman L, Dale A, Kremen WS (2009) Distinct Genetic Influences on Cortical Surface Area and Cortical Thickness. Cereb Cortex 19: 2728–2735.

Panizzon MS, Fennema-Notestine C, Kubarych TS, Chen C-H, Eyler LT, Fischl B, Franz CE, Grant MD, Hamza S, Jak A, Jernigan TL, Lyons MJ, Neale MC, Prom-Wormley EC, Seidman L, Tsuang MT, Wu H, Xian H, Dale AM, Kremen WS (2012) Genetic and environmental influences of white and gray matter signal contrast: A new phenotype for imaging genetics? NeuroImage 60: 1686–1695.

Paul LK, Brown WS, Adolphs R, Tyszka JM, Richards LJ, Mukherjee P, Sherr EH (2007) Agenesis of the corpus callosum: genetic, developmental and functional aspects of connectivity. Nat Rev Neurosci 8:287–299.

Paul LK (2011) Developmental malformation of the corpus callosum: a review of typical callosal development and examples of developmental disorders with callosal involvement. J Neurodev Disord 3:3–27.

Pfefferbaum A, Sullivan EV, Carmelli D (2001) Genetic regulation of regional microstructure of the corpus callosum in late life. Neuroreport 12:1677–1681.

Pfefferbaum A, Adalsteinsson E, Sullivan EV (2003) Replicability of diffusion tensor imaging measurements of fractional anisotropy and trace in brain. J Magn Reson Imaging 18:427–433.

Pujol J, Vendrell P, Junqué C, Martí-Vilalta JL, Capdevila A (1993) When does human brain development end? Evidence of corpus callosum growth up to adulthood. Annals of Neurology 34:71–75.

Raffelt D, Tournier J-D, Fripp J, Crozier S, Connelly A, Salvado O (2011) Symmetric diffeomorphic registration of fibre orientation distributions. NeuroImage 56:1171–1180.

Raffelt D, Tournier J-D, Rose S, Ridgway GR, Henderson R, Crozier S, Salvado O, Connelly A (2012) Apparent Fibre Density: A novel measure for the analysis of diffusion-weighted magnetic resonance images. NeuroImage 59:3976–3994.

Rajapakse JC, Giedd JN, Rumsey JM, Vaituzis AC, Hamburger SD, Rapoport JL (1996) Regional MRI measurements of the corpus callosum: a methodological and developmental study. Brain and Development 18:379–388.

Rohlfing T, Rademacher MH, Pfefferbaum A (2008) Volume Reconstruction by Inverse Interpolation: Application to Interleaved MR Motion Correction. In: Medical Image Computing and Computer-Assisted Intervention – MICCAI 2008, pp. 798–806.

Rueckert D, Sonoda LI, Hayes C, Hill DLG, Leach MO, Hawkes DJ (1999) Nonrigid Registration Using Free-Form Deformations: Application to Breast MR Images. IEEE Trans Med Imag 18:712–721.

Schmitt JE, Lenroot RK, Wallace GL, Ordaz S, Taylor KN, Kabani N, Greenstein D, Lerch JP, Kendler KS, Neale MC, Giedd JN (2008) Identification of Genetically Mediated Cortical

Networks: A Multivariate Study of Pediatric Twins and Siblings. Cereb Cortex 18:1737–1747.

Shrout PE, Fleiss JL (1979) Intraclass correlations: Uses in assessing rater reliability. Psychological Bulletin 86:420–428.

Sowell ER, Thompson PM, Tessner KD, Toga AW (2001) Mapping Continued Brain Growth and Gray Matter Density Reduction in Dorsal Frontal Cortex: Inverse Relationships during Postadolescent Brain Maturation. J Neurosci vol 21:8819–8829.

Sullivan EV, Pfefferbaum A (2006) Diffusion tensor imaging and aging. Neuroscience & Biobehavioral Reviews 30:749–761.

Thompson PM, Giedd JN, Woods RP, MacDonald D, Evans AC, Toga AW (2000) Growth patterns in the developing brain detected by using continuum mechanical tensor maps. Nature 404:190–193.

Thompson PM, Cannon TD, Narr KL, van Erp T, Poutanen V-P, Huttunen M, Lönnqvist J, Standertskjöld-Nordenstam C-G, Kaprio J, Khaledy M, Dail R, Zoumalan CI, Toga AW (2001) Genetic influences on brain structure. Nat Neurosci 4:1253–1258.

Tournier J-D, Calamante F, Gadian D-G, Connelly A (2004) Direct estimation of the fiber orientation density function from diffusion-weighted MRI data using spherical deconvolution. NeuroImage 23:1176–1185.

Tournier J-D, Calamante F, Connelly A (2007) Robust determination of the fibre orientation distribution in diffusion MRI: Non-negativity constrained super-resolved spherical deconvolution. NeuroImage 35:1459–1472.

Tournier J-D, Yeh C-H, Calamante F, Cho K-H, Connelly A, Lin C-P (2008) Resolving crossing fibres using constrained spherical deconvolution: Validation using diffusion-weighted imaging phantom data. NeuroImage 42:617–625.

Tournier J-D, Calamante F, Connelly A (2012) MRtrix: Diffusion tractography in crossing fiber regions. International Journal of Imaging Systems and Technology 22:53–66.

Tristán-Vega A, Westin C-F, Aja-Fernández S (2009) Estimation of fiber Orientation Probability Density Functions in High Angular Resolution Diffusion Imaging. NeuroImage 47:638–650.

Tristán-Vega A, Westin C-F, Aja-Fernández S (2010) A new methodology for the estimation of fiber populations in the white matter of the brain with the Funk–Radon transform. NeuroImage 49:1301–1315.

Tuch DS, Reese TG, Wiegell MR, Makris N, Belliveau JW, Wedeen VJ (2002) High angular resolution diffusion imaging reveals intravoxel white matter fiber heterogeneity. Magnetic Resonance in Medicine 48:577–582.

Tuch DS (2004) Q-ball imaging. Magnetic Resonance in Medicine 52:1358–1372.

Tustison NJ, Avants BB, Cook PA, Zheng Y, Egan A, Yushkevich PA, Gee JC (2010) N4ITK: Improved N3 Bias Correction. IEEE Transactions on Medical Imaging 29:1310–1320.

Tzourio-Mazoyer N, Landeau B, Papathanassiou D, Crivello F, EtardO, Delcroix N, Mazoyer B, Joliot M (2002) Automated Anatomical Labeling of Activations in SPM Using a Macroscopic Anatomical Parcellation of the MNI MRI Single-Subject Brain. NeuroImage 15:273–289.

Vollmar C, O'Muircheartaigh J, Barker GJ, Symms MR, Thompson P, Kumari V, Duncan JS, Richardson MP, Koepp MJ (2010) Identical, but not the same: Intra-site and inter-site reproducibility of fractional anisotropy measures on two 3.0T scanners. NeuroImage 51:1384–1394.

Wakana S, Caprihan A, Panzenboeck MM, Fallon JH, Perry M, Gollub RL, Hua K, Zhang J, Jiang H, Dubey P, Blitz A, van Zijl P, Mori S (2007) Reproducibility of quantitative

tractography methods applied to cerebral white matter. NeuroImage 36:630–644.

Wedeen VJ, Hagmann P, Tseng W-YI, Reese TG, Weisskoff RM (2005) Mapping complex tissue architecture with diffusion spectrum magnetic resonance imaging. Magnetic Resonance in Medicine 54:1377–1386.

Winkler AM, Kochunov P, Blangero J, Almasy L, Zilles K, Fox PT, Duggirala R, Glahn DC (2010) Cortical thickness or grey matter volume? The importance of selecting the phenotype for imaging genetics studies. NeuroImage 53:1135–1146.

Wozniak JR, Lim KO (2006) Advances in white matter imaging: A review of in vivo magnetic resonance methodologies and their applicability to the study of development and aging. Neuroscience & Biobehavioral Reviews 30:762–774.

Zaitsev M, Hennig J, Speck O (2004) Point spread function mapping with parallel imaging techniques and high acceleration factors: Fast, robust, and flexible method for echo-planar imaging distortion correction. Magnetic Resonance in Medicine 52:1156–1166.

Zhan L, Leow AD, Aganj I, Lenglet C, Sapiro G, Yacoub E, Harel N, Toga AW, Thompson PM (2011) Differential information content in staggered multiple shell HARDI measured by the tensor distribution function. In: 2011 IEEE International Symposium on Biomedical Imaging: From Nano to Macro, pp. 305–309.
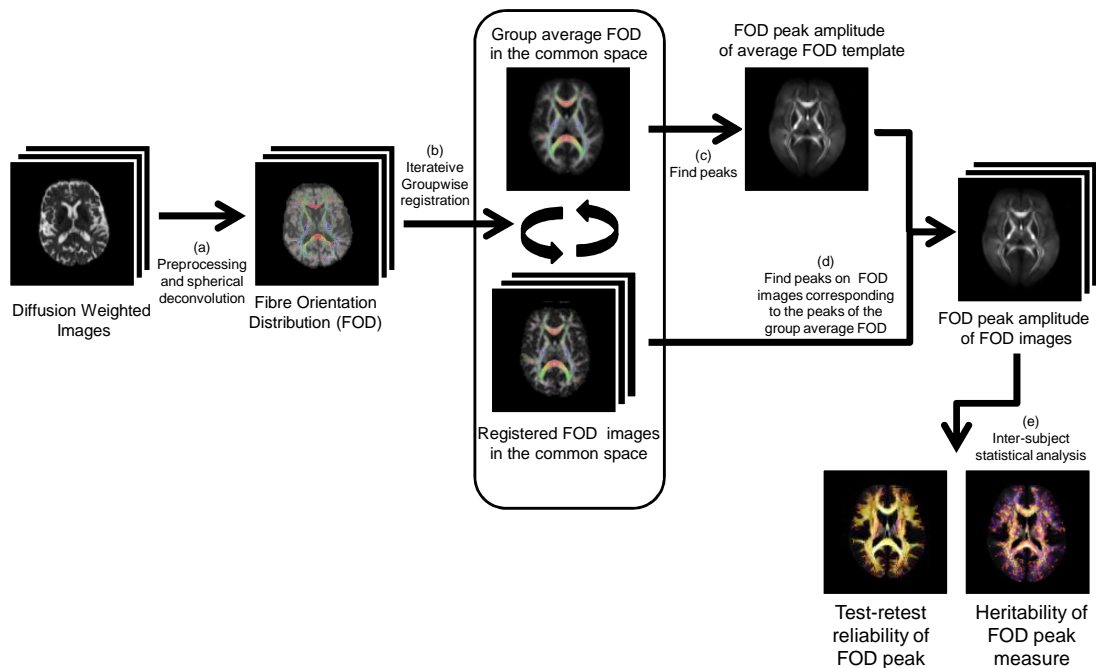
Figure 1. The preprocessing steps for the Diffusion Weighted Images (DWIs) include spatial normalization, FOD peak measurement, and inter-subject statistical analysis: (a) In preprocessing, the DWIs were corrected for bias field effects, motion and eddy current artifacts, and then used to reconstruct the Fibre Orientation Distribution (FOD) image by spherical deconvolution (Tourier *et al*., 2008). (b) FOD images were then spatially normalized into a common atlas space by iterative group-wise registration (Raffelt *et al*., 2012), which produced a group average FOD image template, and the FOD of all the subjects aligned to it. To measure the FOD peaks for each subject, we first (c) identified major FOD peaks on the average template, and then (d) search for FOD peaks on subject FOD images to match the FOD peaks on the template to ensure the correspondence of peak measures across the sample. (e) The inter-subject statistical analysis was then carried out given the FOD peak measurements, thus we were able to evaluate the test-retest reliability of this pipeline by repeated scanned DWIs, and estimate the heritability of FOD peak measurements.
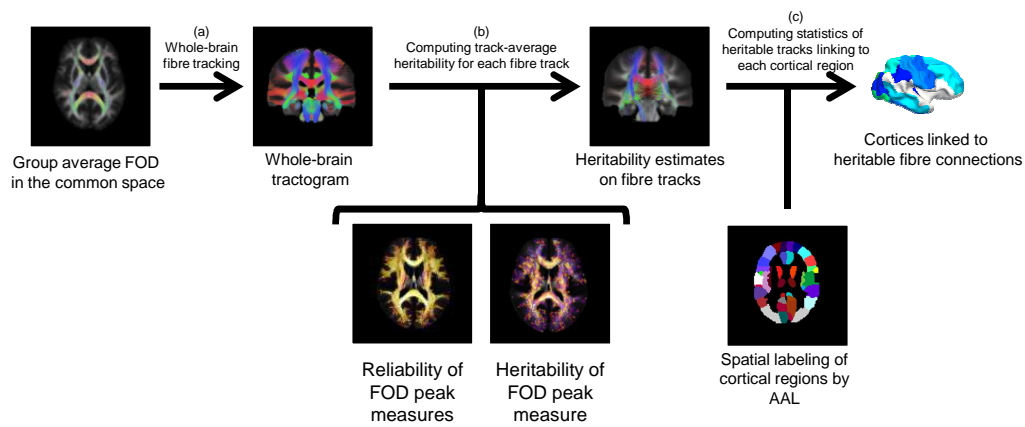
Figure 2. Tract-based analysis of heritability and the identification of cortical regions connected by heritable WM connections. (a) A whole-brain probabilistic fibre-tracking algorithm (Tournier *et al.*, 2012) was used to produce a whole-brain tractogram, which includes the cortico-cortical, cortico-subcortical connections, and fibre tracks connecting the cortex and subcortical nuclei to the brain stem. (b) For individual fibre tracks, the degree of genetic influence at particular locations can be estimated from the heritability of FOD peaks that the fibre is following. For a whole tract, we can compute the average heritability of all sampling points along the whole stretch of the tract. (c) By grouping the tracts by labeling of cortical regions, we identified bundles of fibre tracks connected to a particular cortical region of interest (ROI). The cortical regions are connected by WM fibres with various degrees of heritability.
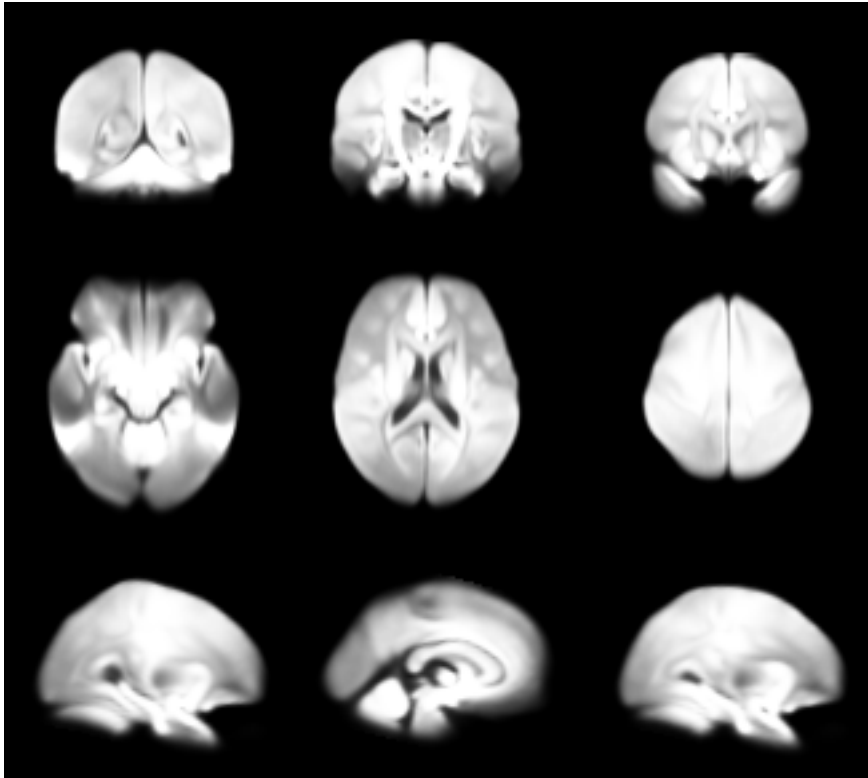
Figure 3: The average of fibre orientation distribution (FOD) images from the sample (*N*=328). The figure shows the component corresponding to the zeroth order spherical harmonic (SH) coefficients of the FOD.
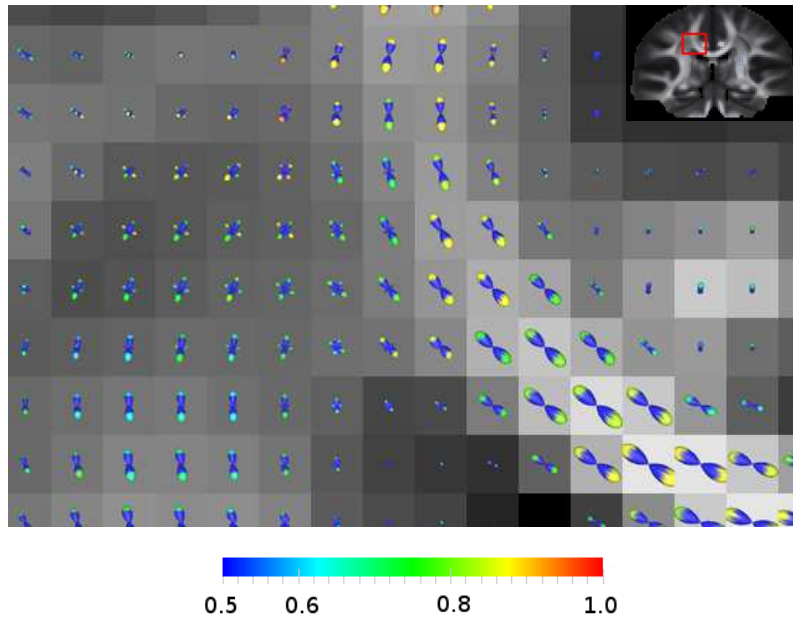
Figure 4. A close-up view of the intra-class correlation (ICC) in fibre orientation distribution (FOD) peak amplitudes, plotted on an average FOD template, with the cap of corresponding peak colour-coded, and overlaid on the fractional anisotropy (FA) map. The body of FOD apart from the peak cap is coloured in blue.
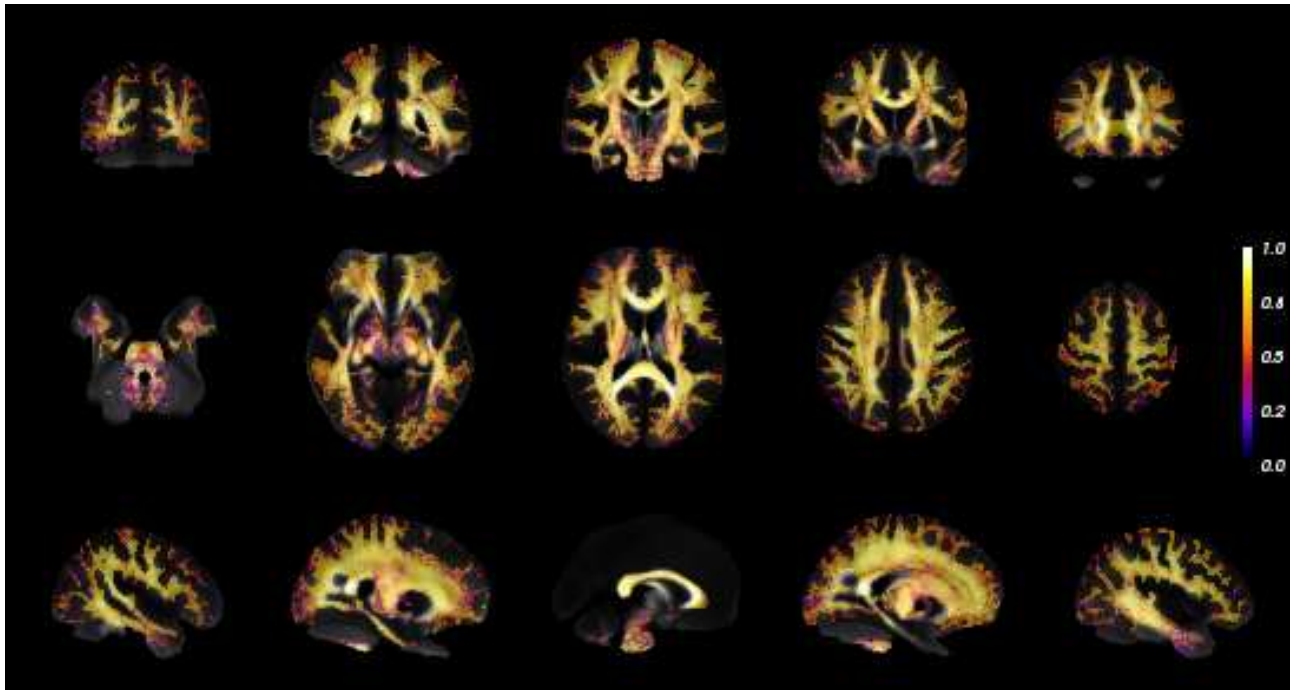
Figure 5: Intraclass correlation (ICC) of the first peak in fibre orientation distribution (FOD) measurement of diffusion MR in white matter region overlaid on the average fractional anisotropy (FA) map.
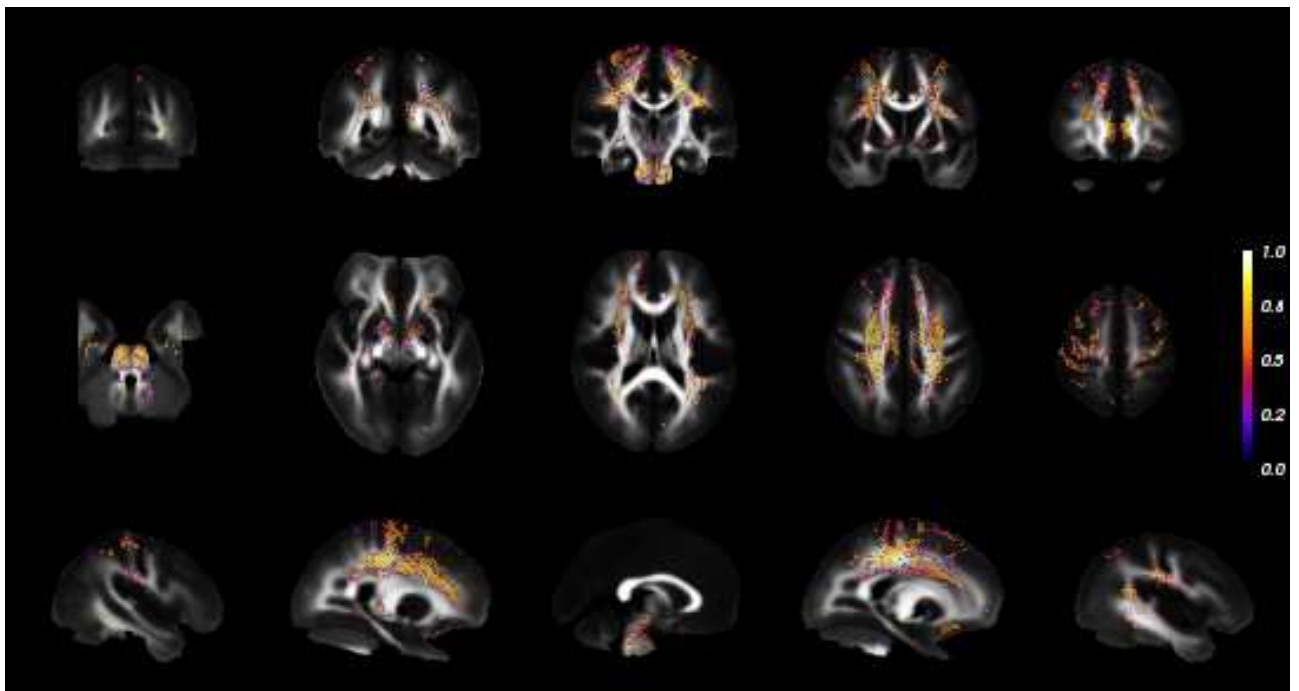
Figure 6: Intraclass correlation (ICC) of the second peak in fibre orientation distribution (FOD) measurement of diffusion MR in white matter region overlaid on the average fractional anisotropy (FA) map. The second peak is identified by threshold with FOD > 0.1.
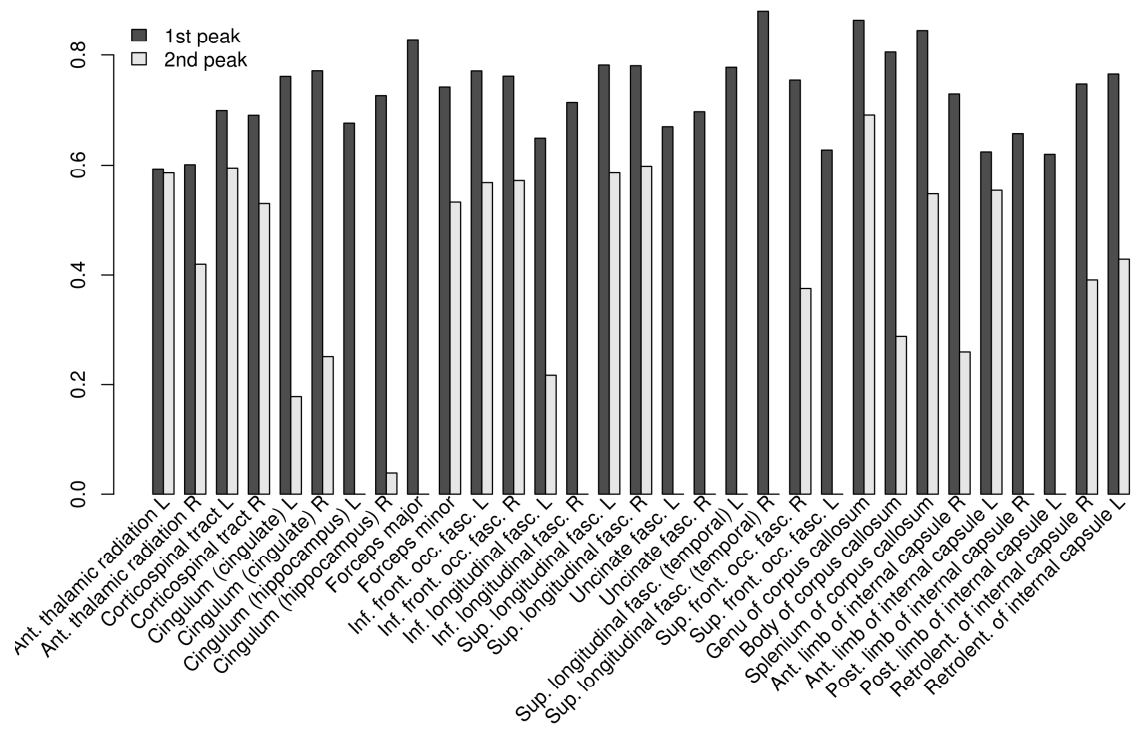
Figure 7: Intraclass correlation (ICC) showing test-retest reliability in fibre orientation distribution (FOD) peak measurements in major white matter tracts and corpus callosum regions of interest (ROIs), as defined by the JHU probabilistic white matter tract atlas and label maps.
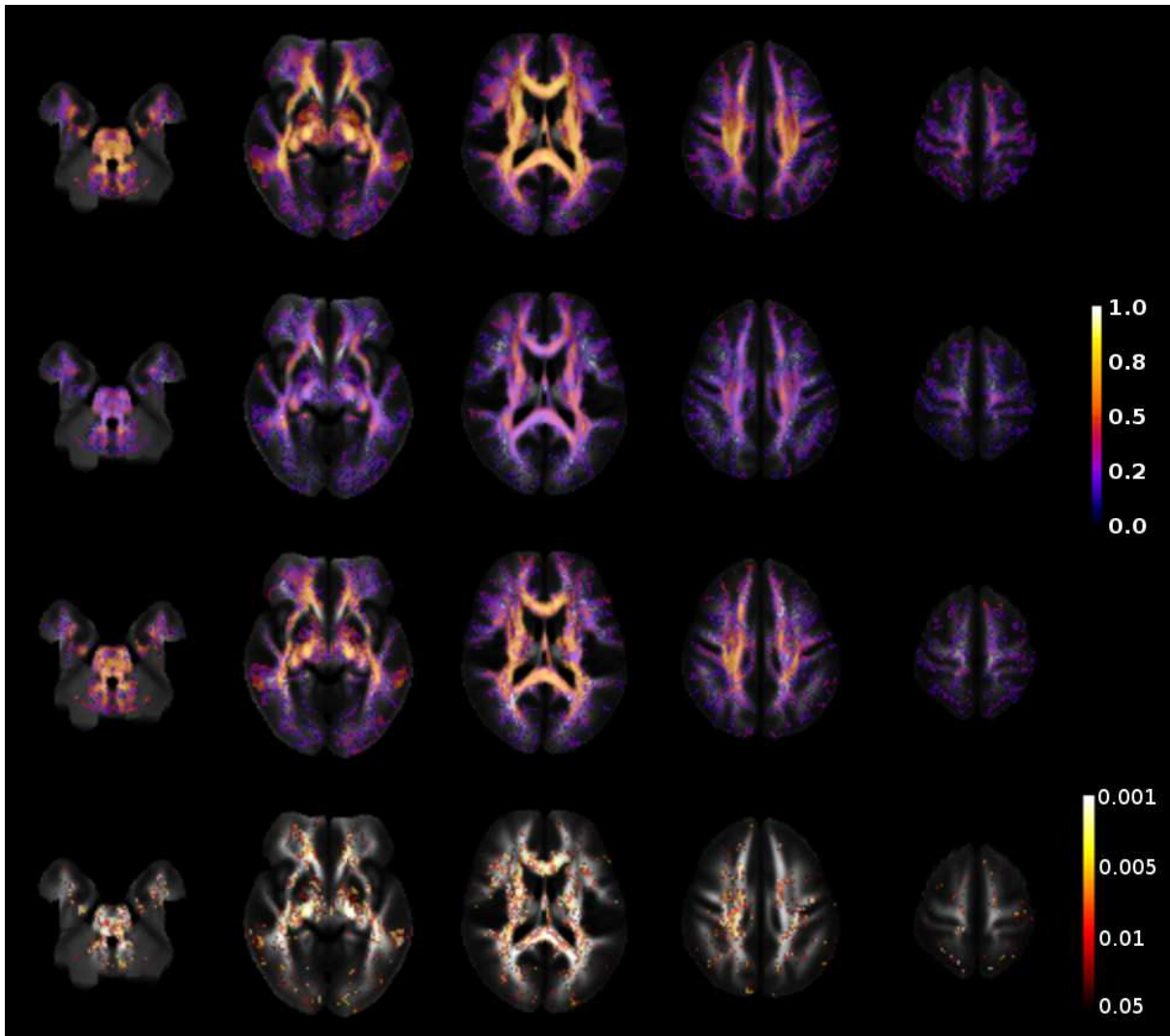
Figure 8: Heritability of the first peak in fibre orientation distribution (FOD) measurement of diffusion MR in white matter overlaid on the average fractional anisotropy (FA) map. From top to bottom: intraclass correlation (ICC) in monozygotic (MZ) twins; ICC in dizygotic (DZ) twins; heritability index h^2; p-value of the additive genetic component by permutation test.
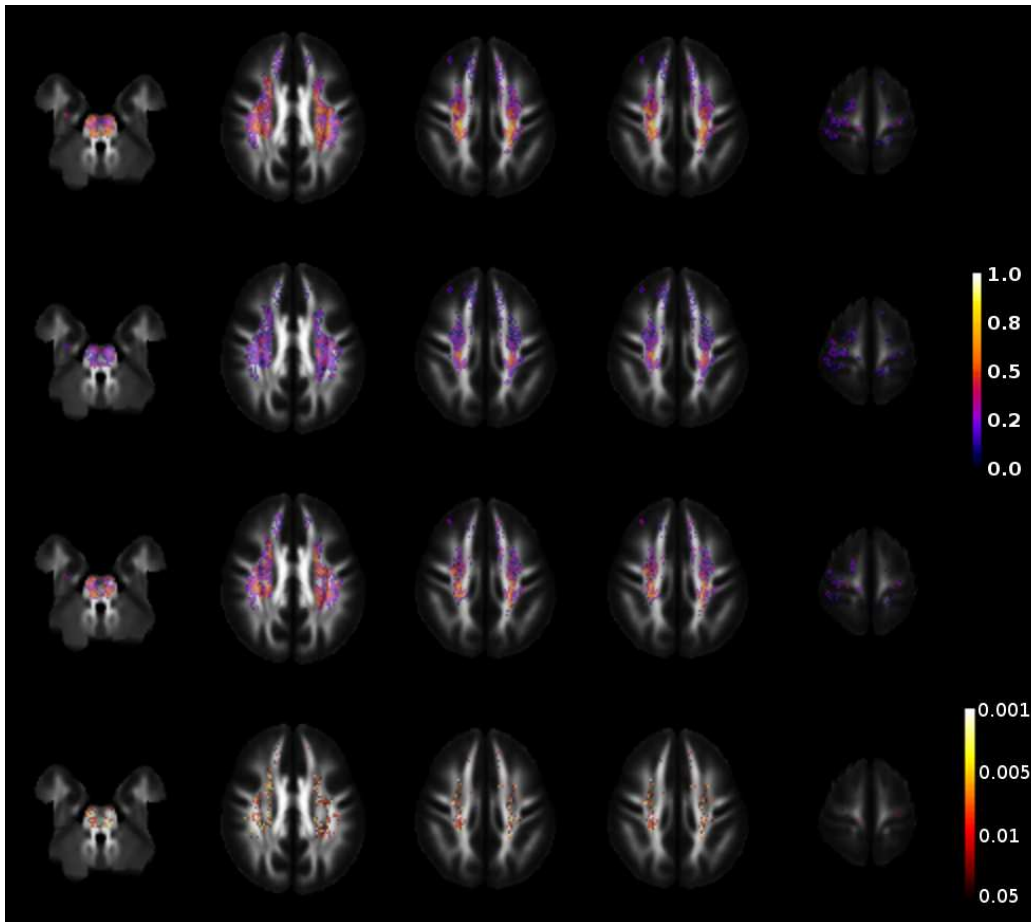
Figure 9: Heritability of the second peak in fibre orientation distribution (FOD) measurement of diffusion MR in white matter voxels with distinct fibre orientations overlaid on the average fractional anisotropy (FA) map. From top to bottom: intraclass correlation (ICC) in monozygotic (MZ) twins; ICC in dizygotic (DZ) twins; heritability index h^2; p-value of the additive genetic component by permutation test.
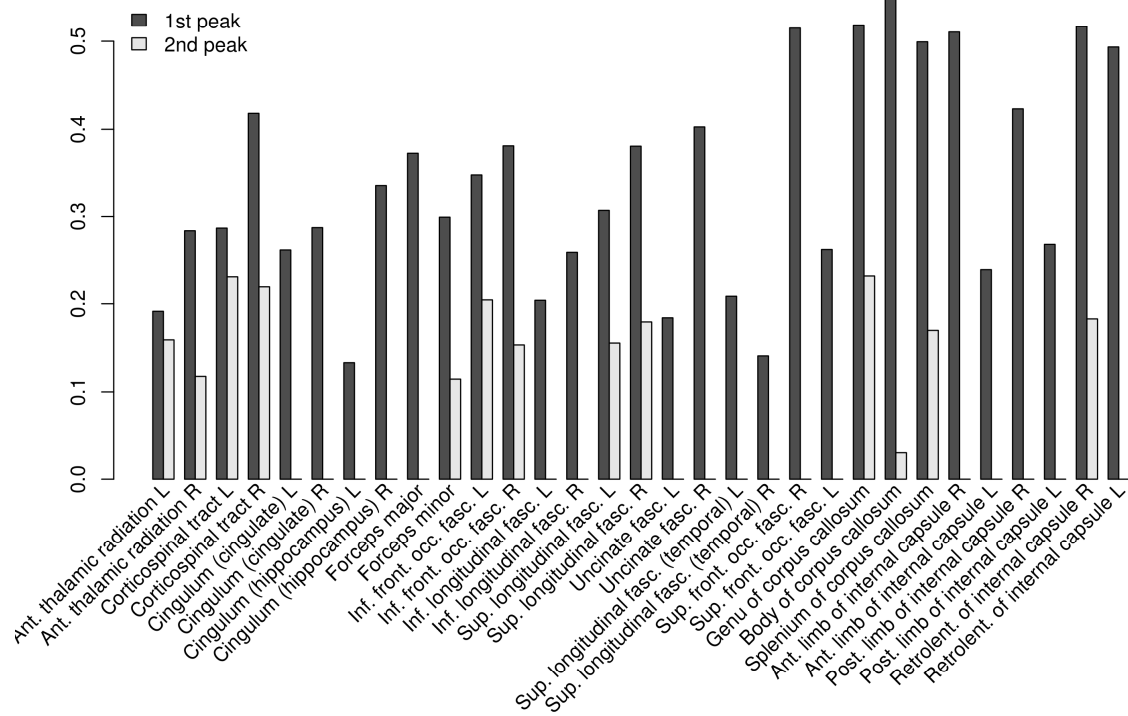
Figure 10: Heritability index (h^2) of fibre orientation distribution (FOD) peak measurements in major white matter tracts and corpus callosum regions of interest (ROIs), as defined by JHU probabilistic white matter tract atlas and label maps.
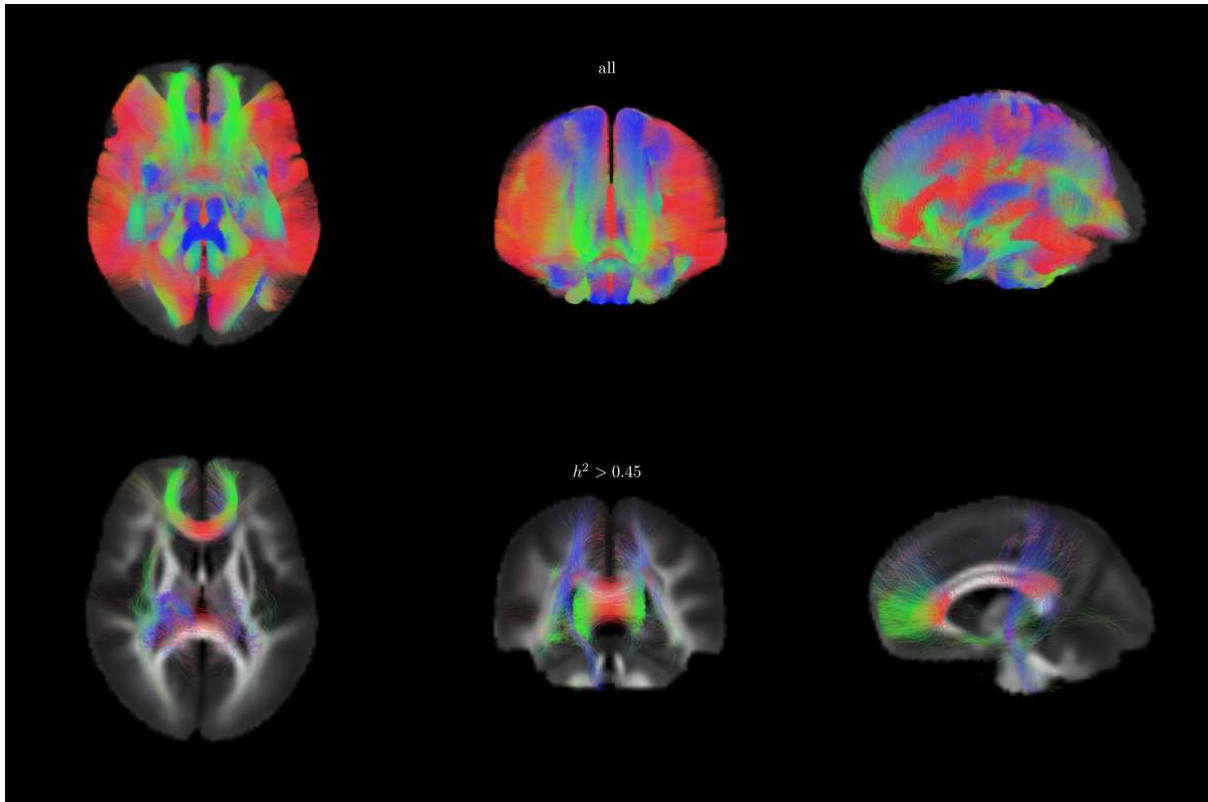
Figure 11: Projections of tractograms produced using a probabilistic tractography algorithm on the average fibre orientation distribution (FOD) map, overlaid on the average FA map. Top: all the tracts with average intraclass correlation (ICC) of test-retest reliability ICC > 0.6; bottom: among the tracts with reliability ICC > 0.6, the tracts with average heritability h^2 > 0.45.
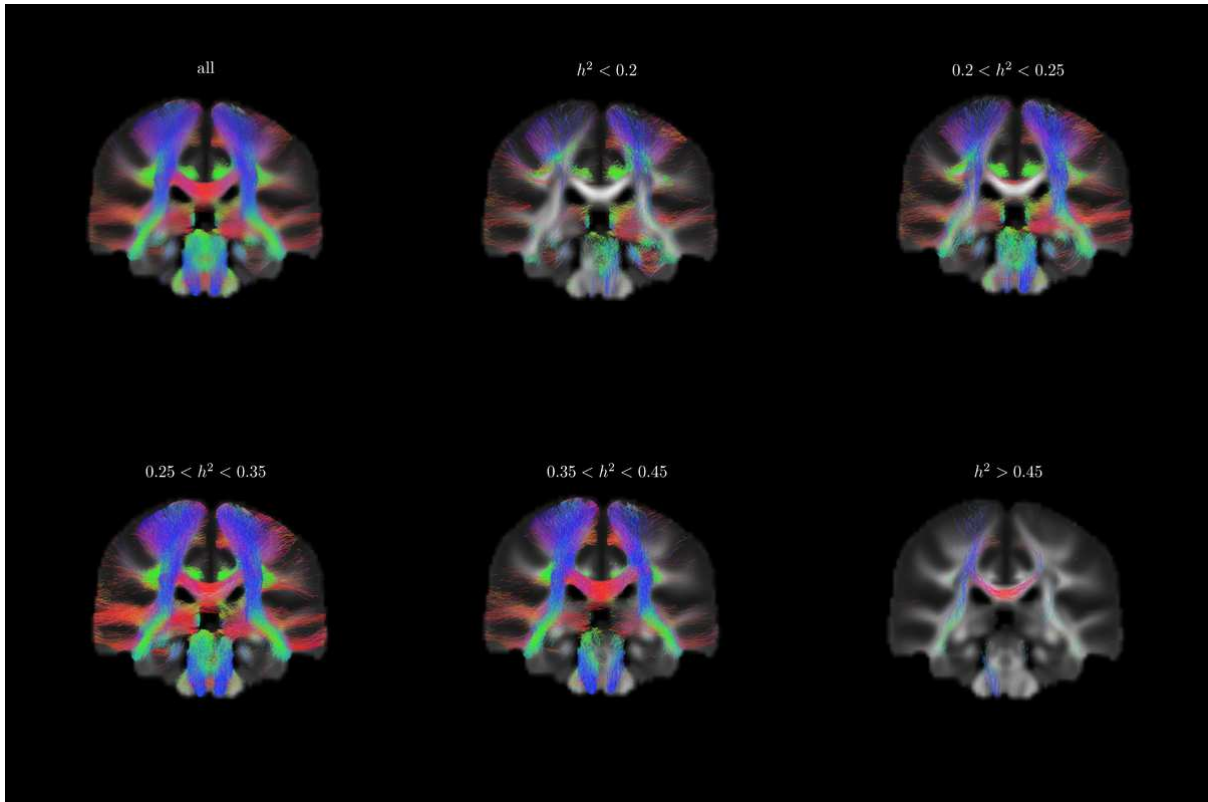
Figure 12: Distribution of fibre tracts (test-retest reliability ICC > 0.6) from the fibre tracking results according to heritability, coronal slice of the tractogram. The sample tracts are separated by thresholding their tract-average heritability index.

(a) mean h^2 of fibre tracts connected to each cortical region

(b) percentage of fibre tracts with heritability greater than 0.3 among all the tracks connected to the cortical region

(c) percentage of fibre tracts with heritability greater than 0.4 among all the tracks connected to the cortical region
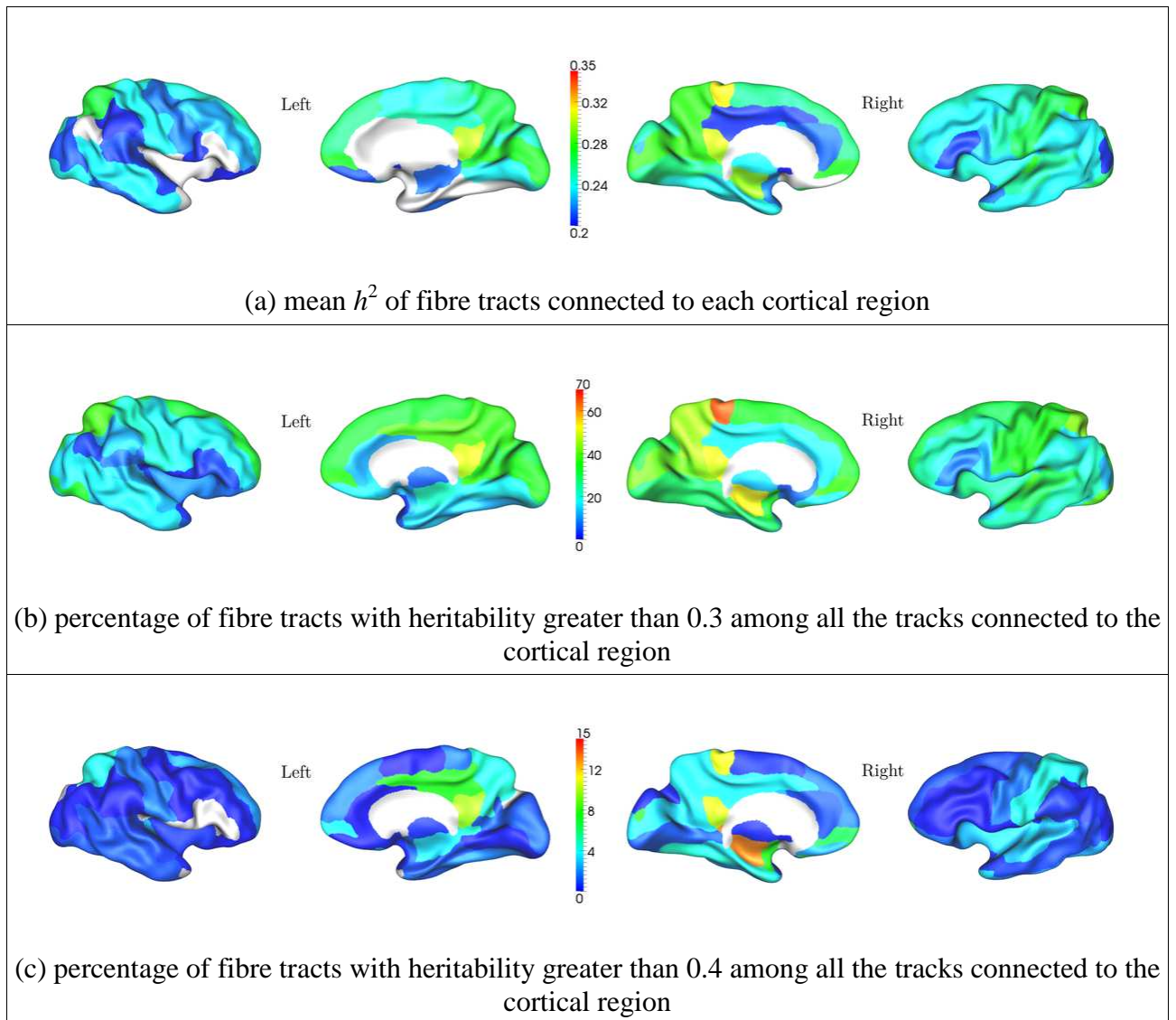
Figure 13: Cortical regions associated with heritable white matter fibres. From top to bottom: (a) mean heritability h^2 of fibre tracts ending in each cortical regions; (b) percentage of tracks connected to each cortical region with $h^2 > 0.3$; (c) $h^2 > 0.4$.

Precentral gyrus (L)	Precentral gyrus (left)	$h^2 < 0.308$ $h^2 > 0.308$
Precentral gyrus (R)	Precentral gyrus (right)	$h^2 < 0.275$ $h^2 > 0.275$
Superior Frontal gyrus (L)	Superior Frontal gyrus dorsolateral (left)	$h^2 < 0.272$ $h^2 > 0.272$
Superior Frontal gyrus (R)	Superior Frontal gyrus dorsolateral (right)	$h^2 < 0.329$ $h^2 > 0.329$

Supplementary motor area (L)		
Supplementary motor area (R)		
Cingulate gyrus (L)		
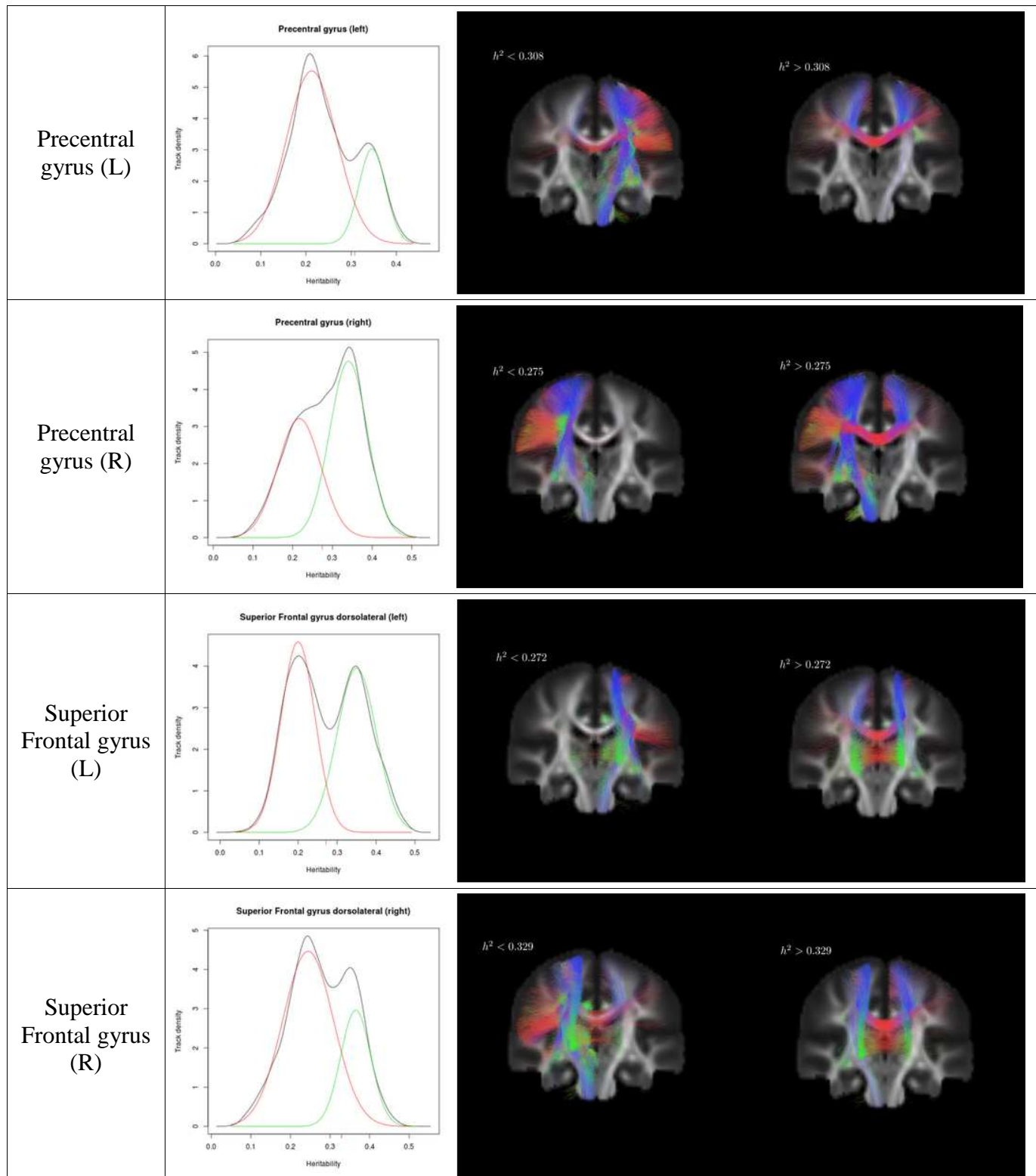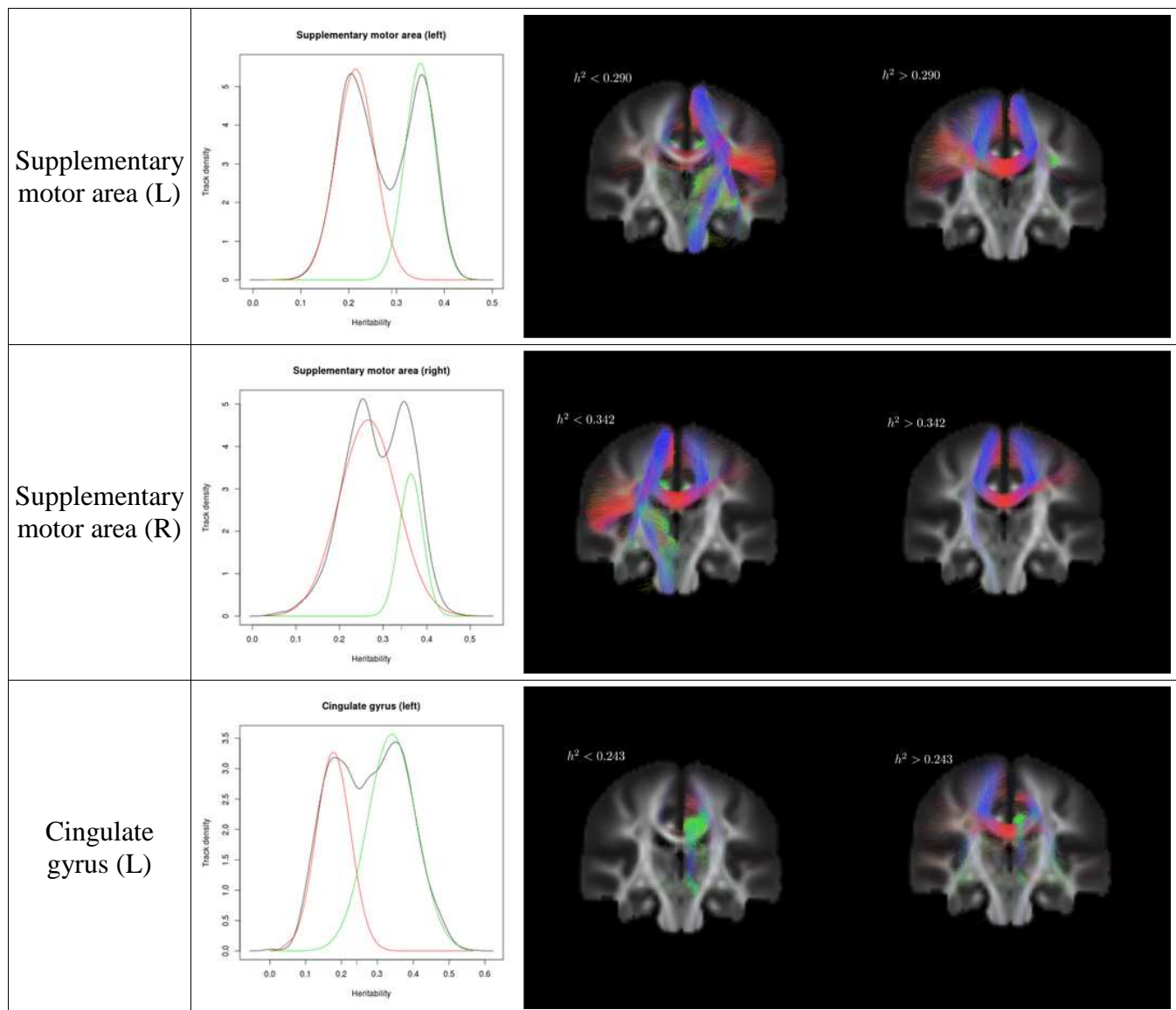
Figure 14: Bimodal distribution of heritability of fibre tracts ending in cortical regions (trimmed average reliability ICC > 0.6). A minimum error threshold (Kittler and Illingworth, 1986) found by fitting bimodal normal distribution (McLachlan and Peel, 2000) was used to separate the fibres with different heritability.